Published in final edited form as:
Magn Reson Med. 2011 June ; 65(6): 1793–1798. doi:10.1002/mrm.22751.

Photoreceptor Degeneration Changes Magnetic Resonance Imaging Features in a Mouse Model of Retinitis Pigmentosa

Qing Wang[1], **Sheng-Kwei Song**[2], **Huiying Zhang**[3], **Bruce A. Berkowitz**[4], **Shiming Chen**[5], **Samuel A. Wickline**[3], and **Junjie Chen**[3,*]

[1]Department of Mechanical Engineering & Materials Science, Washington University, St. Louis, Missouri, USA.

[2]Department of Radiology, Hope Center for Neurological Disorders, Washington University, St. Louis, Missouri, USA.

[3]Department of Medicine, Washington University, St. Louis, Missouri, USA.

[4]Department of Anatomy, Cell Biology, and Ophthalmology, Wayne State University, Detroit, Michigan, USA.

[5]Department of Ophthalmology and Visual Sciences, Washington University, St. Louis, Missouri, USA.

Abstract

Retinal degeneration-1 (*rd1*) mice are animal models of retinitis pigmentosa, a blinding disease caused by photoreceptor cell degeneration. This study aims to determine magnetic resonance imaging (MRI) changes in retinas of 1- and 3-month-old rd1 mice. Apparent diffusion coefficient in retina was measured using diffusion MRI. The blood-retinal barrier leakage was evaluated using gadolinium-diethylenetriaminepentaacetic acid-enhanced T_1-weighted MRI before and after systemic gadolinium-diethylenetriaminepentaacetic acid injection. Photoreceptor degeneration in *rd1* retina was apparent by decreased retinal thickness and loss of water diffusion anisotropy in both 1- and 3-month-old *rd1* mice. Furthermore, statistically significant increase of mean retinal apparent diffusion coefficient and gadolinium-diethylenetriaminepentaacetic acid-enhanced T_1-weighted MRI signals were observed in 3-month-old *rd1* mice comparing with age-matched wild-type mice. Together, these data suggest that MRI parameter changes can signature common pathological changes in photoreceptor-degenerated eyes, particularly blood-retinal barrier leakage-induced retinal edema.

Keywords

rd1; photoreceptor degeneration; blood-retinal barrier; apparent diffusion coefficient; MRI

Retinitis pigmentosa (RP, prevalence 1/4000) is a group of hereditary retinal diseases characterized by progressive photoreceptor cell degeneration. The diagnosis of RP relies upon the clinical history of progressively decreased visual acuity and function. Recent report has assessed cell loss-induced retinal thinning using optical coherence tomography (OCT) (1). Unfortunately, retinal edema, e.g., edematous retinal thickening (2,3), is common in RP patients. Retinal edema alone also causes increase in retinal thickness, which is associated

*Correspondence to: C-TRAIN Group, Campus Box 8215, Washington University School of Medicine, Cortex Building, Suite 101, 4444 Forest Park Ave, St. Louis, MO 63108. junjie@dom.wustl.edu.

with visual loss and morbidity in RP, thus complicating the diagnosis and follow-up of patients with RP.

Clinically, retinal edema in RP has been linked with blood-retinal barrier (BRB) breakdown (4). However, excessive extracellular water accumulation can result from either retinal leakage (i.e., vasogenic retinal edema) or osmotic water movement in the absence of retinal leakage (i.e., cytotoxic retinal edema). At present, it is not clear which mechanism of retinal edema in late stage experimental RP dominates (5). Noninvasive method for specific assessment of vasogenic retinal edema is desired to better understand the disease pathology.

Magnetic resonance imaging (MRI) is a noninvasive method for evaluating BRB leakage and tissue edema in central nervous system. BRB breakdown can be sensitively detected by dynamic contrast-enhanced MRI (DCE-MRI) wherein the leakage of gadolinium-diethylenetriaminepentaacetic acid (Gd-DTPA) into the vitreous results in MR signal enhancement (6). In addition, increased extracellular water content associated with vasogenic tissue edema can also be objectively evaluated by detecting increased apparent diffusion coefficient (ADC) of tissue water using diffusion-weighted MRI (DWI) (7). Our previous results have shown that DWI delineates cell layer-specific ADC in normal retina raising the possibility of using this technique to assess retinal edema associated with RP (8).

In this study, we applied Gd-DTPA-enhanced T_1-weighted (T_1W) MRI and DWI to examine possible MRI manifestations associated with BRB leakage and vasogenic edema in the retinal degeneration-1 (*rd1*) mice. The *rd1* mouse is a well-established animal model of RP (9). The retina of *rd1* mice undergoes rapid photoreceptor cell degeneration from the second postnatal week (10). By 4 weeks of age, nearly all photoreceptor cells have been lost resulting in ~50% decrease of retinal thickness relative to that in age-matched wild-type (WT) mice. The degeneration of photoreceptor cells in *rd1* mice subsequently causes progressive loss of the retinal layer that forms the tight cell–cell junctions of the outer BRB, the retinal pigment epithelium (RPE) (11). In 1–1.5-month *rd1* mice, the first degenerative change of this layer includes flattening of RPE cells into a thin layer without detectable cell loss. By 2 months of age, some RPE cell loss is evident, and RPE cell reduction increased rapidly by 3 month of age (12). Thus, this study was designed to noninvasively reveal additional pathogenic changes as a consequence of RPE cell loss in 1- and 3-month-old *rd1* mice eyes. Our results consistently showed that Gd-DTPA-enhanced T_1W MRI detected BRB breakdown in 3-month-old, but not in 1-month-old *rd1* mice. In addition, DWI detected an increase of retinal ADC in 3-month-old *rd1* mice, suggesting the development of vasogenic retinal edema correlating with the incidence of BRB breakdown. Thus, our results demonstrated MRI signatures in response to vasogenic retinal edema that is independent to the changes in retinal thickness.

MATERIALS AND METHODS

All procedures in this study conformed to the guidelines set forth by Animal Studies Committee of Washington University in St. Louis.

Animal Model

One- and three-month-old male C57BL/6J-*Pdeb*^{rd1} *le*/ *Pdeb*^{rd1} *le* (*rd1*; Jackson lab, Bar Harbor, Marine) and WT C57BL/6 (Harlan Laboratory, Indianapolis, IN) mice were examined (n = 5 for each group). Mice were anesthetized by intraperitoneal injection of ketamine (87 mg/kg) and xylazine (13 mg/kg) followed by constant subcutaneous infusion of ketamine (54 mg/kg/h)/xylazine (4 mg/kg/h). The infusion rate of ketamine/xylazine cocktail for individual mouse was adjusted to maintain the respiratory rate between 150 and 210 breaths/min throughout the experiment. Animal body temperature was maintained at

37°C and monitored using a small animal heating and monitoring system (SA instruments, NY).

MRI Protocol

MRI of the mouse eye was performed on a Varian 11.74T UNITY-INOVA scanner using a custom-built solenoid coil for radio-frequency transmission and signal reception. All images were acquired on a nasal-temporal slice that bisects the eye through the optic nerve head.

A spin-echo diffusion-weighted sequence was performed as previously described (8). Briefly, three orthogonal diffusion gradients were applied in directions: parallel to, and in- and out-of-plane perpendicular to the axis of the optic nerve. In each direction, a pair of diffusion-weighted images was acquired with positive and negative diffusion gradients permitting postprocessing to minimize the background magnetic field gradient effect on the diffusion measurement. Acquisition parameters were: slice thickness 400 μm; field-of-view 6 × 6 mm^2; in-plane resolution 47 × 47 μm^2; data matrix 128 × 128 (zero filled to 256 × 256); number of averages 2; repetition time 1.5 sec; echo time 34 msec; diffusion gradient on time (δ) 5 msec; duration time between two diffusion gradients (Δ) 15 msec; *b*-values 0 and 954 sec/mm^2. All diffusion-weighted images were acquired with respiratory gating.

Gd-DTPA-enhanced T_1W MRI was performed to assess the BRB integrity. Three precontrast T_1W images were acquired before the injection of Gd-DTPA, and the average of vitreous signal intensity was used as the baseline. Subsequently, animals were injected with a single dose of Gd-DTPA (1 mmol/kg) through an intraperitoneal catheter followed by continuous acquisition of fifteen T_1W images in 30 min. Acquisition parameters were: repetition time 1 sec; echo time 16 msec; field-of-view 6 × 6 mm^2; data matrix 128 × 64; in-plane resolution 47 × 94 μm^2; slice thickness 400 μm.

Data Analysis

The segmentation of retinal layers was performed as previously described (Fig. 1) (8). Briefly, the retina/choroid complex was first identified based on its hyperintensity on diffusion-weighted images. After the segmentation of retina/choroid complex, finer segmentation of retinal layers was performed by the MR signal intensity. For WT mice, the choroid and three MR-detected retinal layers (i.e., inner, middle, and outer layer) were identified. For *rd1* mice, the choroid and a single MR-detected retinal layer were identified. The region of interest was defined as a pair of retina segments at each side of the optic nerve for quantifying MRI parameters. The two ends of each segment were ~260 and 790 μm away from the optic nerve. To reduce the partial volume effect from the vitreous, the pixel adjacent to vitreous on zero-filled images (in-plane resolution = 23 × 23 μm^2) was excluded in data analysis. Thus, the analyzed retina layer in *rd1* mice is approximately three pixels thick.

Diffusion-weighted MR images were processed as previously described (8) to determine the mean ADC and two directional components, i.e., ADC$_{\parallel}$ and ADC$_{\perp}$, respectively, in the directions parallel and perpendicular to the optic nerve.

Gd-DTPA-induced vitreous MR signal enhancement was determined using a region of interest covering the entire vitreous space defined on the baseline image and then applied to all postcontrast images. The signal change of each pixel in the region of interest was calculated as $[S(t) - S(0)]/S(0)$, where $S(t)$ is the postcontrast signal intensity at time t and $S(0)$ is the baseline signal intensity. The signal intensity change was measured up to 30 min after Gd-DTPA injection to detect coherent and progressive signal enhancements in the vitreous.

Histology

Animals were euthanized after the conclusion of MRI. Eyes were enucleated and flash-frozen. The frozen eyes were sectioned at 8-μm thick through the optic nerve head and perpendicular to retina. Tissue sections were stained with hematoxylin and eosin (H&E) for morphological analysis of the retina.

Statistics

All statistical analyses were performed using SAS software (SAS Institute, Cary, NC). Quantitative data were expressed as mean ± SD. For comparisons between two experimental groups, the significance of the difference between the means was calculated. Two-way ANOVA was used to test the difference of: (1) ADC|| and ADC⊥ among the inner, middle, and outer layer of WT mice and the remaining retina of *rd1* mice; (2) mean ADC in the inner layer of WT mice and the remaining retina of *rd1* mice at 1 and 3 months of age; (3) Vitreous signal enhancement of *rd1* and WT mice at each time point after Gd-DTPA injection. When an overall significance of $P < 0.05$ was attained by ANOVA, comparisons between the means were performed using the Freeman–Tukey test.

RESULTS

DWI-Detected Photoreceptor Cell Degeneration in *rd1* Mice

Figure 1 shows MR and histology images of the retina of WT and *rd1* mice. The retina/choroid complex was hyperintense on diffusion-weighted images in all mice. The reduced thickness of retina/choroid complex in *rd1* mice due to the degeneration of photoreceptor cells is visually apparent. Nondiffusion-weighted images identified multiple signal intensity layers in the retina/choroid complex (Fig. 1). Based on our previous observations in WT mice (8), the outmost bright MR-detected layer is assigned to the choroid in both WT and *rd1* mice. Thus, three MR-detected retinal layers, i.e., inner (dark), middle (bright), and outer (dark) layers, were observed in WT mice. In contrast, only a single MR-detected retinal layer exhibiting dark signal intensity was observed in *rd1* mice.

Figure 2 shows the quantified ADC|| and ADC⊥ in each MR-detected retinal layer of *rd1* and WT mice. ADC|| was ~2-fold higher than ADC⊥ ($P < 0.05$) in the outer retinal layer of WT mice. In contrast, ADC|| was comparable with ADC⊥ in the inner retinal layer of WT mice. Comparable ADC|| and ADC⊥ were also observed in the *rd1* mouse retina reflecting the loss of diffusion anisotropy after the degeneration of parallel aligned photoreceptor cells.

The mean ADC of all MR-detected retinal layers of WT mice exhibited no statistically significant difference between first and third month of age (Fig. 3). However, mean ADC in the remaining retina of *rd1* mice increased ~ 30% from 1–3 months of age, suggesting a possible late development of retinal edema in 3-month-old *rd1* mice.

Gd-DTPA-Enhanced T_1W MRI Detected BRB Breakdown in 3-Month-Old *rd1* Mice

Gd-DTPA-enhanced T_1W MRI was performed to assess BRB breakdown as a potential cause of the increased mean retinal ADC in 3-month-old *rd1* mice. Thirty minutes after systemic injection of Gd-DTPA, no apparent increase in vitreous MR signal was observed for 1-month-old *rd1* mice or any WT mice (Fig. 4A,B). In contrast, a substantial increase of MR signal was observed in the vitreous of 3-month-old *rd1* mice at 10 min after Gd-DTPA infusion that progressively diffuses to the entire posterior vitreous cavity (Fig. 4C), a clear sign of BRB breakdown. At 30 min after Gd-DTPA treatment, the extent of vitreous signal enhancement was significantly higher in 3-month-old *rd1* mice (37 ± 7%) than that of 1-month-old *rd1* and WT mice (~ 10%; $P < 0.05$).

DISCUSSION

In this study, in vivo MRI was applied to assess retinal degeneration and remodeling in *rd1* mice. Diffusion MRI detected reduction in retinal thickness, and loss of water diffusion anisotropy resulting from photoreceptor cell degeneration. In vivo measurements allow objectively mapping the temporal evolution of the mean retinal ADC and changes of vitreous signal intensity following systemic Gd-DTPA injection to visualize vasogenic retinal edema following photoreceptor degeneration. These data highlight the potential of in vivo MRI to detect photoreceptor cell loss and the resultant edema in retinal degenerative models.

The MR-detected retinal layers in WT mice were assigned according to our previous report where histology and MR-detected thickness of corresponding layers were compared. The MR-detected inner, middle, and outer retinal layers in WT mice (Fig. 1e and h) were tentatively assigned to nerve fiber layer/ganglion cell layer/inner plexiform layer (NFL/GCL/IPL), inner nuclear layer/outer plexiform layer (INL/OPL), and photoreceptor cell outer nuclear layer/inner segment/outer segment (ONL/IS/OS) as previously described (8). Because of the degeneration of photoreceptor cells in *rd1* mice, histology determined retinal thickness were 91 ± 5 μm and 80 ± 1 μm at first and third month of age, respectively. Thus, the used 47-μm in-plane resolution of MR image was insufficient to accurately resolve the retinal layer thickness in *rd1* mice. The single MR-detected dark retinal layer in *rd1* mice was tentatively assigned to NFL/GCL/IPL, because ADC$_{\parallel}$ is comparable with ADC$_{\perp}$ in this remaining retina layer. The bright INL/OPL was not identifiable from the adjacent bright choroid after the loss of photoreceptor cells. The current tentative assignment of the remaining *rd1* retinal layer as NFL/GCL/IPL based on diffusion MRI property is also consistent with that determined functionally using manganese-enhanced MRI (13) in 3-month-old *rd1* mice.

Photoreceptor degeneration leads to BRB breakdown in both experimental (12) and clinical (14) subjects. In the present study, the integrity of BRB was assessed in vivo using Gd-DTPA-enhanced T_1W MRI, a noninvasive MRI technique sensitive to BRB breakdown-induced vascular leakage (15). Thirty minutes after Gd-DTPA infusion, vitreous T_1W signal in 1-month-old *rd1* mice and all WT mice increased by ~10% consistent with previously reported values (16). In contrast, ~40% increase of vitreous T_1W signal was observed in 3-month-old *rd1* mice. At the concentrations expected in the vitreous, the T_1W signal is a linear function of vitreous Gd-DTPA (15), and so the increased T_1W signal in 3-month-old *rd1* mice is consistent with BRB damage and leakage of Gd-DTPA into the vitreous (6).

BRB breakdown leads to fluid accumulation in the interstitial space of retina causing retinal edema impairing retinal function in RP (3). However, the diagnosis of vasogenic retinal edema in most clinical and experimental RP subjects is complicated by the progressive cell degeneration-induced retinal thinning. Previous studies in the central nervous system diseases have demonstrated vasogenic tissue edema can be detected by correlating ADC increase and coexisting blood-tissue barrier breakdown (17). In the present study, both retinal ADC increase and BRB breakdown were detected in 3-month-old *rd1* mice suggesting the presence of vasogenic retinal edema. In contrast, the absence of retinal Gd-DTPA leakage in 1-month-old *rd1* mice, as well as no statistical significant difference of mean ADC between the remaining retina of 1-month-old *rd1* mice and the corresponding inner MR-detected retinal layer of age-matched WT mice, argues against vasogenic retinal edema at this time point. The observed low diffusion anisotropy in the retina of 1-month-old *rd1* mice, as demonstrated by comparable ADC$_{\parallel}$ and ADC$_{\perp}$, is likely a function of less organized inner retinal cell structure than that of controls, instead of vasogenic edema. Unfortunately, validating the presence of vasogenic retinal edema based on retinal

thickening in 3-month-old *rd1* mice is difficult, because the *rd1* mouse retina undergoes progressive loss of inner retinal neuron cells that may lead to retinal thinning. This work sets the stage for additional studies to correlate the increased ADC with BRB breakdown-induced retinal thickness change to evaluate the sensitivity and the specificity of increased ADC and BRB breakdown as markers of vasogenic retinal edema.

OCT has been widely used in both clinical and animal research due to its high resolution and rapid imaging. Kim et al. (18) showed that the spectral-domain OCT may be used to monitor the progression of retinal degeneration in *rd1* mice. Ruggeri et al. (19) also used high resolution OCT system to obtain 3D view of retinal layers in rhodopsin knockout mice, a model for photoreceptor degeneration. Despite its extremely high spatial resolution in vivo, OCT does not distinguish edema from cell swelling within the retina nor provide information on BRB integrity. In addition, the potential of OCT to detect vasogenic retinal edema-induced retinal thickening in RP is limited because of the concurrent retinal thinning. Compared with OCT, MRI possesses unique advantages to delineate cellular organization, cell injury, blood perfusion, and neuron activity. Combining these thickness independent measures with OCT may provide novel opportunity to more accurately assess the underlying pathology in retinal diseases.

One practical limitation of the *rd1* model used in this study is the difficulty of choosing an early time point before 1 month of age of *rd1* mice. An early time point would demonstrate the progressive nature of the degeneration. We had tried and failed to image younger pups to demonstrate the “early detection” capability of MRI in retina pathology. Specifically, the mouse retina is not fully developed at birth. The photoreceptor inner and outer segments in WT mice develop between the second and third postnatal weeks. The photoreceptor degeneration in *rd1* mice started from the second postnatal week, which overlaps with the postnatal development of photoreceptor cells. This makes it difficult, if not impossible, to choose an early time point to demonstrate the existence of progressive photoreceptor degeneration of *rd1* and WT mice before the changes begin.

In summary, our results on *rd1* mice highlighted DWI and Gd-DTPA-enhanced T_1W MRI signatures in response to retinal degeneration. Well-validated MRI markers may be used to characterize the mechanisms underlying retinal edema formation in vivo. These MRI methods may be further applied to longitudinally evaluate the progression of retinal remodeling in other animals models of slow retinal degeneration. Finally, the MRI signatures described herein may benefit the development of novel therapeutic approaches on retinal degeneration and edema.

Acknowledgments

This study is supported by NIH (Chen J, Chen S, Berkowitz, BA, and Song S.-K.), Washington University DRTC Pilot and Feasibility Grant (Chen J), Juvenile Diabetes Research Foundation (Berkowitz, BA); NIH Animal Models of Diabetic Complications Consortium and Mouse Metabolic Phenotyping Centers Pilot and Feasibility Programs (Berkowitz, BA), and unrestricted grants from Research to Prevent Blindness to Washington University Department of Ophthalmology and Visual Science and to Wayne State University Kresge Eye Institute.

Grant sponsor: NIH; Grant numbers: R21 EY018914, R01 EY012543, R01 EY018109, R01 NS NS054194, P01 NS 059560; Grant sponsor: Washington University DRTC Pilot and Feasibility Grant; Grant number: 5 P60 DK20579; Grant sponsor: Juvenile Diabetes Research Foundation; Grant sponsor: NIH Animal Models of Diabetic Complications Consortium and Mouse Metabolic Phenotyping Centers Pilot and Feasibility Programs; Grant sponsor: Washington University Department of Ophthalmology and Visual Science (Research to Prevent Blindness); Grant sponsor: Wayne State University Kresge Eye Institute.

REFERENCES

1. Witkin AJ, Ko TH, Fujimoto JG, Chan A, Drexler W, Schuman JS, Reichel E, Duker JS. Ultra-high resolution optical coherence tomography assessment of photoreceptors in retinitis pigmentosa and related diseases. Am J Ophthalmol. 2006; 142:945–952. [PubMed: 17157580]
2. Sandberg MA, Brockhurst RJ, Gaudio AR, Berson EL. The association between visual acuity and central retinal thickness in retinitis pigmentosa. Invest Ophthalmol Vis Sci. 2005; 46:3349–3354. [PubMed: 16123439]
3. Hajali M, Fishman GA. The prevalence of cystoid macular oedema on optical coherence tomography in retinitis pigmentosa patients without cystic changes on fundus examination. Eye (Lond). 2009; 23:915–919. [PubMed: 18425064]
4. Fishman GA, Fishman M, Maggiano J. Macular lesions associated with retinitis pigmentosa. Arch Ophthalmol. 1977; 95:798–803. [PubMed: 860943]
5. Bringmann A, Reichenbach A, Wiedemann P. Pathomechanisms of cystoid macular edema. Ophthalmic Res. 2004; 36:241–249. [PubMed: 15583429]
6. Berkowitz BA, Roberts R, Luan H, Peysakhov J, Mao X, Thomas KA. Dynamic contrast-enhanced MRI measurements of passive permeability through blood retinal barrier in diabetic rats. Invest Ophthalmol Vis Sci. 2004; 45:2391–2398. [PubMed: 15223822]
7. Schaefer PW, Buonanno FS, Gonzalez RG, Schwamm LH. Diffusion-weighted imaging discriminates between cytotoxic and vasogenic edema in a patient with eclampsia. Stroke. 1997; 28:1082–1085. [PubMed: 9158653]
8. Chen J, Wang Q, Zhang H, Yang X, Wang J, Berkowitz BA, Wickline SA, Song SK. In vivo quantification of T1, T2, and apparent diffusion coefficient in the mouse retina at 11.74T. Magn Reson Med. 2008; 59:731–738. [PubMed: 18383302]
9. Chang B, Hawes NL, Hurd RE, Davisson MT, Nusinowitz S, Heckenlively JR. Retinal degeneration mutants in the mouse. Vision Res. 2002; 42:517–525. [PubMed: 11853768]
10. LaVail MM, Mullen RJ. Role of the pigment epithelium in inherited retinal degeneration analyzed with experimental mouse chimeras. Exp Eye Res. 1976; 23:227–245. [PubMed: 976367]
11. Marc RE, Jones BW, Watt CB, Strettoi E. Neural remodeling in retinal degeneration. Prog Retin Eye Res. 2003; 22:607–655. [PubMed: 12892644]
12. Neuhardt T, May CA, Wilsch C, Eichhorn M, Lutjen-Drecoll E. Morphological changes of retinal pigment epithelium and choroid in rd-mice. Exp Eye Res. 1999; 68:75–83. [PubMed: 9986744]
13. Ivanova E, Roberts R, Bissig D, Pan Z, Berkowitz BA. Retinal channelrhodopsin-2-mediated activity in vivo evaluated with manganese-enhanced magnetic resonance imaging. Mol Vis. 2010; 16:2059–1067.
14. Spalton DJ, Bird AC, Cleary PE. Retinitis pigmentosa and retinal oedema. Br J Ophthalmol. 1978; 62:174–182. [PubMed: 638111]
15. Berkowitz, BA. MRI studies of blood-retinal barrier: new potential for translation of animal results to human application. In: Joussen, AM.; Gardner, TW.; Kirchhof, B.; Ryan, SJ., editors. Retinal vascular diseases. Springer; Berlin: 2007. p. 154-164.
16. Kolodny NH, Freddo TF, Lawrence BA, Suarez C, Bartels SP. Contrast-enhanced magnetic resonance imaging confirmation of an anterior protein pathway in normal rabbit eyes. Invest Ophthalmol Vis Sci. 1996; 37:1602–1607. [PubMed: 8675403]
17. Kuroiwa T, Nagaoka T, Ueki M, Yamada I, Miyasaka N, Akimoto H, Ichinose S, Okeda R, Hirakawa K. Correlations between the apparent diffusion coefficient, water content, and ultrastructure after induction of vasogenic brain edema in cats. J Neurosurg. 1999; 90:499–503. [PubMed: 10067919]
18. Kim KH, Puoris'haag M, Maguluri GN, Umino Y, Cusato K, Barlow RB, de Boer JF. Monitoring mouse retinal degeneration with high-resolution spectral-domain optical coherence tomography. J Vis. 2008; 8:17, 11–11. [PubMed: 18318620]
19. Ruggeri M, Wehbe H, Jiao S, Gregori G, Jockovich ME, Hackam A, Duan Y, Puliafito CA. In vivo three-dimensional high-resolution imaging of rodent retina with spectral-domain optical coherence tomography. Invest Ophthalmol Vis Sci. 2007; 48:1808–1814. [PubMed: 17389515]

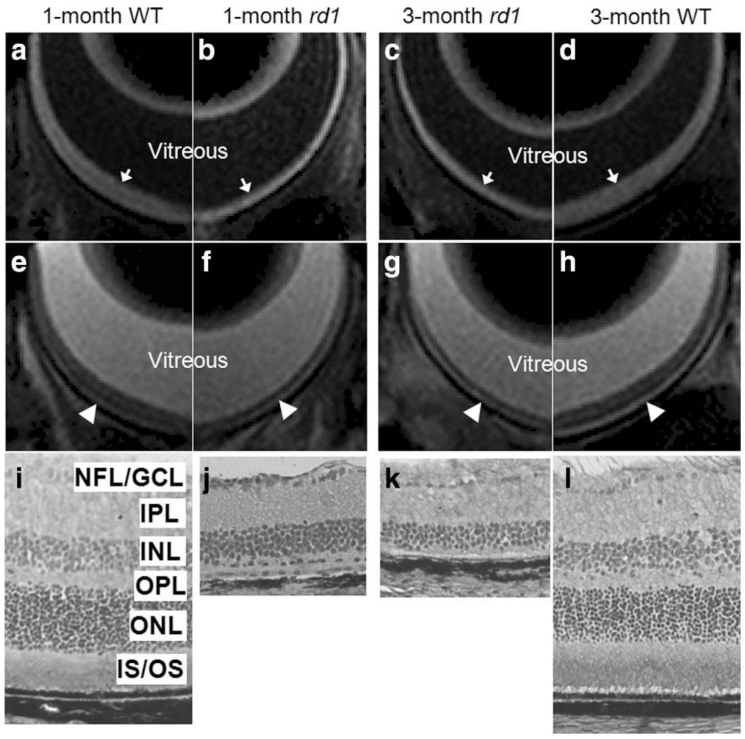

FIG. 1.

Representative diffusion-weighted images of the eyes of 1- and 3-month-old *rd1* mice and age-matched wild-type mice (**a–d**). The retina/choroid complex (arrows) was hyperintense on all diffusion-weighted images. Nondiffusion-weighted images of the same mouse eyes show three MR-detected retinal layers, exhibiting dark (inner)—bright (middle)—dark (outer) signal intensity in wild-type and a single dark MR-detected retinal layer in *rd1* retina (**e–h**). Arrow heads indicates the bright choroid layer. H&E stained slices of wild-type and *rd1* mouse retinas show the absence of photoreceptor cells in *rd1* mice (**i–l**).

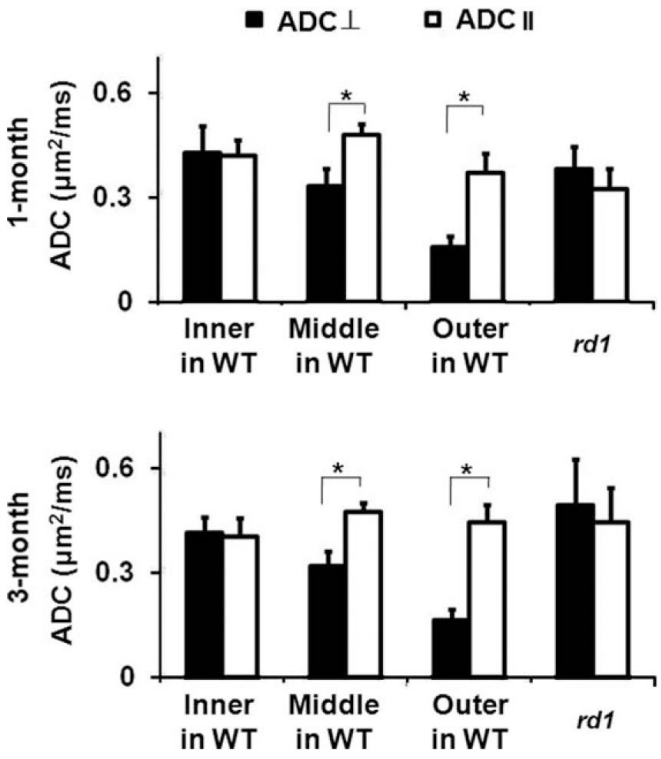

FIG. 2.

ADC|| and ADC⊥ in respective retinal layers of wild-type and the remaining layer of *rd1* mice were determined at first (**a**) and third month (**b**) of age. *, $P < 0.05$.

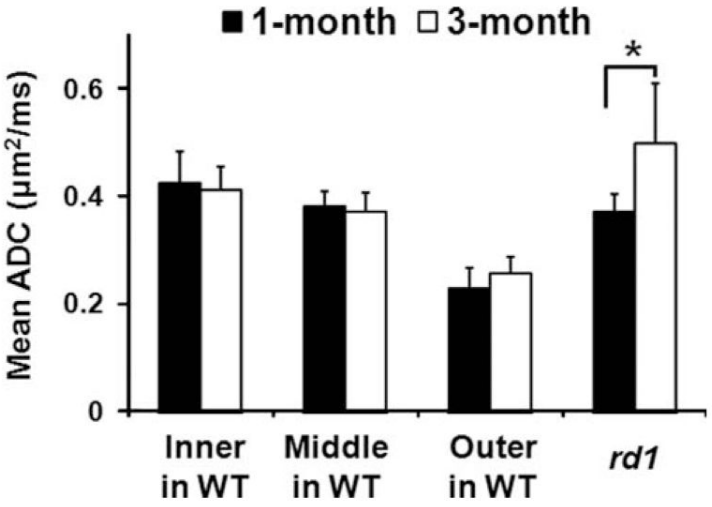

FIG. 3.

DWI determined mean ADC in the remaining retina of *rd1* mice and in all MR-detected layers of wild-type mouse at of first and third month of age. *, $P < 0.05$. Mean ADC in three MRI-detected retinal layers of wild-type are comparable at the age of first and third month. The mean ADC of 3-month-old *rd1* is significantly higher than that in 1-month-old *rd1*, but both are within the control range for the MR-detected inner layer of the same age WT.

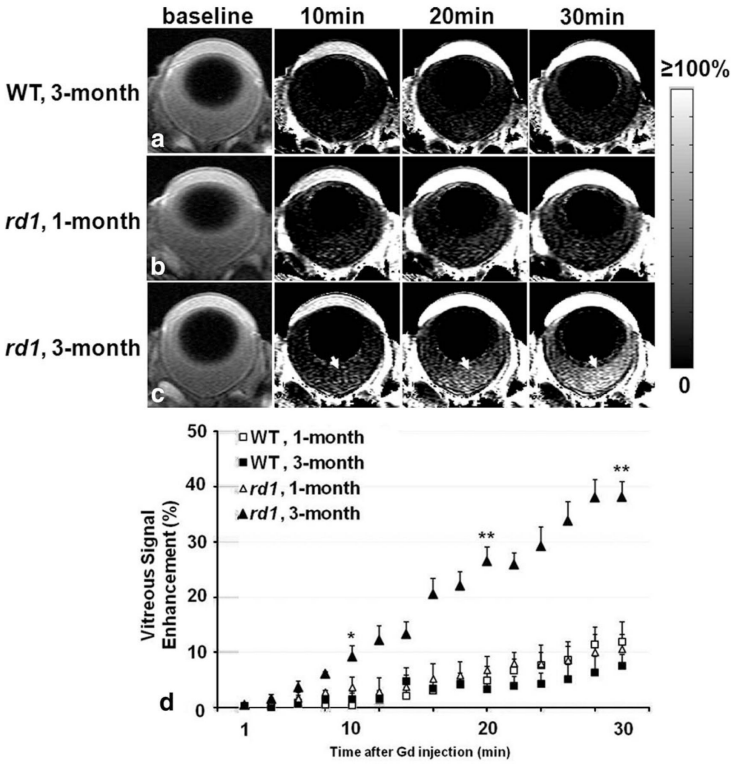

FIG. 4.

Representative MR images of the eyes of a 3-month-old WT, 1- and 3-month-old *rd1* mice at baseline and T_1W signal enhancement in the same eyes at 10, 20, and 30 min after intraperitoneal injection of Gd-DTPA (**a–c**). Quantitative analysis shows that the vitreous signal in 3-month-old *rd1* mice increases monotonically after Gd-DTPA injection and is ~40% higher than the baseline value at 30 min (**d**). In contrast, only around 10% vitreous signal enhancement was observed in 1-month-old *rd1* mice and all WT mice. *, $P < 0.05$ compared with 1-month-old *rd1* mice and all WT mice at 10 min; **, $P < 0.005$ compared with 1-month-old *rd1* mice and all WT mice at 20 min and all time points after that.